Comparison of Characterization Methods for Assessing the Temperature Dependencies of Elastic and Piezoelectric Constants of Piezoelectric Materials

Ailing Xiao, Liguo Tang, Shanshan Sun, Songji Wu, Xinye Wu, and Wenyu Luo

***Abstract*— The accurate characterization of the temperature dependencies (TD) of the full tensorial properties of piezoelectric materials (PMs) makes it possible to predict the performance of electromechanical devices fabricated using PMs at different temperatures. The electric resonance (ER) and the resonant ultrasound spectroscopy (RUS) methods—used to characterize the TD of the elastic and piezoelectric constants (EPCs) of PMs—are systematically compared by characterizing Fuji C-213 lead zirconate titanate ceramics. Five samples must be used in ER; however, RUS needs one sample only. Therefore, the preparation of ER samples requires time that is approximately five times higher than that of the RUS sample. Moreover, the temperature-dependent ER measurement requires times that are more than three times than that required by the RUS measurement. RUS can only characterize samples with a high-mechanical quality factor, which should be greater than several hundred. RUS takes more time than ER on data processing. Most material constants characterized using RUS are consistent with those characterized using ER. Overall, RUS can obtain more accurate EPCs than ER, which is proved by comparing the measured electric impedance spectra with those calculated using the ER and RUS results. ER has been extensively used to characterize PMs, and however, RUS has not, due to the lack of commercial RUS software for PMs. It is very difficult to develop. This study provides a reference for the selection of various methods for characterizing the TD of the EPCs of PMs. Moreover, it may facilitate the development of RUS for characterizing PMs.**

***Index Terms*— Characterization, elastic and piezoelectric constants (EPCs), electric resonance (ER) method, piezoelectric materials (PMs), resonant ultrasound spectroscopy (RUS).**

NOMENCLATURE

Notation	Description
ε^{T}	Free dielectric constant.
ε^{S}	Clamped dielectric constant.
k_{31}	Transverse or lateral coupling factor.
k_{33}	Longitudinal coupling factor.
k_{15}	Shear coupling factor.
k_t	Thickness coupling factor.
k_P	Planar coupling factor.
s^{E}	Elastic compliance under constant electric field.
s^{D}	Elastic compliance under constant electric displacement.
c^{E}	Elastic stiffness under constant electric field.
c^{D}	Elastic stiffness under constant electric displacement.
d	Piezoelectric strain constant.
e	Piezoelectric stress constant.

I. INTRODUCTION

PIEZOELECTRIC materials (PMs) are extensively used to fabricate electromechanical devices that operate at various temperatures. For example, the piezoelectric transducers used in some nuclear reactors for monitoring the accelerator-driven systems should withstand elevated temperatures (up to 450 °C) [1].

The temperature dependencies (TD) of the full tensorial properties of PMs are of great interest to PM and electromagnetic device manufacturers because temperature has a significant influence on the properties and performance of these materials and devices.

Three types of methods have been developed to characterize the TD of elastic and piezoelectric constants (EPCs) of PMs, i.e., electric resonance (ER), resonant ultrasound spectroscopy (RUS), and electric impedance spectroscopy (EIS). The TD of dielectric constants $\varepsilon_{ii}^{\mathrm{T}}$ and ε_{ii}^{S} $(i = 1, 2, 3)$ can be determined

Manuscript received 22 March 2023; revised 13 June 2023; accepted 10 July 2023. Date of publication 26 July 2023; date of current version 7 August 2023. This work was supported in part by the National Natural Science Foundation of China under Grant 12274358 and Grant U22A2012, and in part by the Open Fund of State Key Laboratory of Acoustics under Grant SKLA202309. The Associate Editor coordinating the review process was Dr. Kamel Haddadi. *(Corresponding authors: Liguo Tang; Xinye Wu.)*

Ailing Xiao, Shanshan Sun, and Songji Wu are with the Key Laboratory of Underwater Acoustic Communication and Marine Information Technology, Ministry of Education, College of Ocean and Earth Sciences, Xiamen University, Xiamen 361005, China (e-mail: alxiao@stu.xmu.edu.cn; sssun@stu.xmu.edu.cn; wusji@stu.xmu.edu.cn).

Liguo Tang is with the Key Laboratory of Underwater Acoustic Communication and Marine Information Technology, Ministry of Education, College of Ocean and Earth Sciences, Xiamen University, Xiamen 361005, China, also with the State Key Laboratory of Acoustics, Institute of Acoustics, Chinese Academy of Sciences, Beijing 100045, China, and also with Southern Marine Science and Engineering Guangdong Laboratory (Zhuhai), Zhuhai 519000, China (e-mail: liguotang@xmu.edu.cn).

Xinye Wu is with the School of Architecture and Civil Engineering, Xiamen University, Xiamen 361005, China (e-mail: wuxinye@xmu.edu.cn).

Wenyu Luo is with the State Key Laboratory of Acoustics, Institute of Acoustics, Chinese Academy of Sciences, Beijing 100045, China, and also with the University of Chinese Academy of Sciences, Beijing 101408, China (e-mail: lwy@mail.ioa.ac.cn).

Digital Object Identifier 10.1109/TIM.2023.3298668

using a dielectric spectrometer. The ultrasonic pulse-echo (UPE) method is often used as an auxiliary tool for ER and RUS. Some elastic stiffness constants, for example, c_{11}^{E} and c_{33}^{D}, can be characterized using UPE. The major notations used in this article are listed in the Nomenclature.

ER is suggested by the Institution of Electrical and Electronic Engineers (IEEE) Standard on piezoelectricity [2]. Multiple resonators must be prepared for ER characterization, including thickness extensional (TE), thickness shear extensional (TSE), length extensional (LE), length thickness extensional (LTE), and radial extensional (RE) resonators. Therefore, the preparation of the ER samples is tedious and time-consuming. Moreover, different resonators should satisfy different size requirements. For example, a TE resonator should satisfy $l_x \gg l_z$ and $l_y \gg l_z$, where l_x, l_y, and l_z are the sizes of the resonator along the x-, y-, and z-directions, respectively. The z-direction is the poling direction. To satisfy the size requirement, some piezoelectric resonators are very thin because it is difficult to prepare large samples with high homogeneity for some PMs, such as relaxor-based single crystals and $Bi_4Ti_3O_{12}$ ceramics. Large errors may occur during the measurement of resonance and antiresonance frequencies when the thin sample is fixed by the impedance test fixture because the force applied on the surface of the thin samples cannot be neglected. However, the equations used in the ER method were derived under homogeneous boundary conditions. In addition to the size requirement, to obtain reliable results, the multiple samples used in the ER and UPE methods must have high homogeneity; otherwise, sample-to-sample variation is too large to be neglected.

In other words, the EPCs obtained using ER may be inconsistent if the multiple samples used in the measurement are not homogeneous, the size requirement of the resonators is not satisfied, or very thin samples are fixed by the impedance test fixture during the measurement. For example, Shanthi et al. [3] obtained inconsistent full matrix constants of $[011]_c$ poled PMN-PT single crystals using ER [3], [4]. Moreover, the self-consistency problem may worsen at elevated temperatures.

There are many published articles on the elastic and piezoelectric properties of different PMs characterized using the ER and UPE methods at room temperature [5], [6], [7], [8], [9], [10]. However, for the aforementioned reasons, the published TD findings of the elastic and piezoelectric properties are scarce compared with the characterization of PMs at room temperature using ER and UPE. For example, to the best of our knowledge, there is only one publication on the characterization of the TD of all EPCs of relaxor-based single crystals using ER [11]. Qiao et al. [12] characterized the TD of EPCs of [001]-poled rhombohedral $Pb(In_{1/2}Nb_{1/2})O_3$-$Pb(Mg_{1/3}Nb_{2/3})O_3$-$PbTiO_3$ (PIN-PMN-PT) single crystals using ER; however, only partial elastic constants were characterized. The ER method has been used to characterize the TD of the elastic and piezoelectric properties of lead zirconate titanate (PZT) ceramics by Zhuang et al. [13] from −269 °C to 26.8 °C, by Sheritt et al. [14] from 0 °C to 100 °C, and by Sabat et al. [15] from −165 °C to 195 °C. Li et al. [16] characterized the TD of the piezoelectric constant d_{33} of PZT using ER from 20 °C to 300 °C. Moreover, the ER method was used to characterize the TD of the elastic and piezoelectric properties of $BaTiO_3$ ceramics from 10 °C to 80 °C [17], lithium tantalate and lithium niobate single crystals from 0 °C to 110 °C [18], $Bi_2ZnB_2O_7$ crystals from −150 °C to 150 °C [19], and $Pb(Mg_{1/3}Nb_{2/3})O_3$–$PbZrO_3$–$PbTiO_3$ ferroelectric single crystals at 30 °C, 50 °C, and 100 °C [11]. These studies are listed in Table I.

Methods based on a single sample must be developed to overcome the shortcomings of characterization methods based on multiple samples. RUS is one of these techniques. The principle of RUS is given as follows. The resonance frequencies of a solid sample are determined by its geometrical sizes and material properties; the material properties of the sample can be determined from its resonance frequencies after its geometrical sizes are known. RUS has often been used to characterize the elastic constants of elastic materials and their TD [20], [21], [22]. Compared with published reports on the TD of elastic constants of elastic samples characterized using RUS, those on the TD of EPCs of piezoelectric samples characterized using RUS are limited. Tarumi et al. [23] characterized the low-temperature EPCs of $LiNbO_3$ and $LiTaO_3$ single crystals using RUS. Tang and Cao characterized the TD of the elastic and piezoelectric properties of PZT-4 [24] and the $[001]_c$ poled Mn-doped 24PIN–46PMN–30PT single crystal [25] using RUS. Hu et al. [26] characterized the TD of the elastic and piezoelectric properties of $BaTiO_3$ ceramics. Fenu et al. [27] characterized the full tensorial constants of Pb-free $Na_{1/2}Bi_{1/2}TiO_3$ ceramics at ambient temperature using ER, based on which their TD was characterized from the ambient temperature to 80 °C using RUS. These studies are also listed in Table I.

In recent years, another method based on a single sample, i.e., EIS, was developed to characterize the TD of the full matrix constants of PMs [28]. However, the reliability of EIS has not been proved by sufficient published results. Moreover, this method is time-consuming because the electric impedance spectrum of the piezoelectric sample should be repeatedly computed many times using the finite element method (FEM) during the inversion.

ER has been extensively used to determine the EPCs of PMs [4], [5], [6], [7], [8], [9], [10], [11], [12], [13], [14], [15], [16], [17]; however, RUS has not. The reason for this phenomenon is probably the fact that the commercial RUS software for PMs has not been available yet and is very difficult to develop. In theory, both ER and RUS can characterize the TD of the EPCs of piezoelectric samples. Consequently, the following questions arise. First, which method can obtain more precise results? Second, which method is more efficient? Third, are there limitations to ER and RUS? Answering these questions is important for the selection of characterization methods for different PMs. The choice of method may determine the success or failure of the characterization. Moreover, it will facilitate the development of new characterization techniques for PMs, such as RUS. Note that the characterization techniques for the TD of EPCs of PMs are very few.

TABLE I
PUBLISHED STUDIES ON THE CHARACTERIZATION OF TD OF MATERIAL CONSTANTS OF PMs

Authors	Material	Method	Characterized constants	Temperature
Zhuang *et al.* [13]	Pure PZT	ER	s_{11}^{E}, d_{31}, k_{31}, d_{33}, k_{33}	-269 °C – 26.8 °C
Sheritt *et al.* [14]	PZT–4D	ER	Complete set[a]	0 °C – 100 °C
Sabat *et al.* [15]	Soft and hard PZT	ER	Complete set	-165 °C – 195 °C
Li *et al.* [16]	PZT5, PZT-5H and PZT8	ER	d_{33}, k_{33}	20 °C – 300 °C
Marutake and Ikeda [17]	$BaTiO_3$	ER	s_{11}^{E}, s_{33}^{E}, s_{44}^{E}, d_{31}, d_{33}	10 °C – 80 °C
Smith and Welsh [18]	$LiNbO_3$ and $LiTaO_3$	UPE and ER	Complete set	0 °C – 110 °C[b]
Qiao *et al.* [12]	[001]-Poled PIN-PMN-PT	ER	Complete set	-10 °C – 70 °C
Chen *et al.* [19]	$Bi_2ZnB_2O_7$	ER	Complete set	-150 °C – 150 °C
Zhang *et al.* [11]	PMN–PZT	ER	Complete set	30 °C, 50 °C, 100 °C
Tarumi *et al.* [23]	$LiNbO_3$ and $LiTaO_3$	RUS	Complete set	-267 °C – 3 °C
Tang and Cao [24]	PZT–4	RUS	Complete set	20 °C – 120 °C
Tang *et al.* [25]	Mn-doped 24PIN–46PMN–30PT	RUS	Complete set	25 °C – 55 °C
Hu *et al.* [26]	$BaTiO_3$	RUS	Complete set	20 °C – 80 °C
Fenu *et al.* [27]	$Na_{1/2}Bi_{1/2}TiO_3$	RUS	Complete set	20 °C – 80 °C
Bouchy *et al.* [28]	$LiNbO_3$	EIS	Complete set	25 °C – 900 °C
Present work	Fuji C-213 PZT	ER and RUS	Complete set	20 °C – 110 °C

[a] Complete set of elastic and piezoelectric constants.

[b] The TD of elastic and piezoelectric constants were computed on the basis of the temperature derivative.

However, to date, there have been no published reports comparing ER and RUS based on reliable experimental results. To clarify the aforementioned questions, the TD of the EPCs of Fuji C-213 PZT was characterized using these two methods in this study. PZT is the most extensively used PM. The Fuji C-213 PZT is a type of hard PZT, which has a high-mechanical quality factor (Q_M) of 2500. It can be characterized not only by ER but also by RUS. Moreover, the ER method was compared with the RUS method in detail based on the characterization procedures and results.

The rest of this article is organized as follows. Section II presents the preparation of the ER and RUS samples, the measurement of dielectric constants and electric impedance curves, the principles of ER and RUS, and the RUS setup. Section III presents the results characterized using ER and RUS, the TD of the dielectric constants, the assessment of the characterization results, and the comparison of ER and RUS. Section IV concludes this article.

II. MATERIALS AND METHODS

A. Preparation of Samples

Fig. 1 shows the samples used in ER and RUS. All samples are rectangular parallelepipeds except the RE resonator. The samples were prepared using the C-213 PZT of Fuji Ceramics Corporation. Its density (ρ) was determined using the Archimedes method to be equal to 7772 kg/m^3. The matrices of its elastic stiffness constant $\mathbf{c}^{E}$, piezoelectric stress constant $\mathbf{e}$, and clamped dielectric constant ε^{S} are formulated as

$$\mathbf{c}^{E} = \begin{bmatrix} c_{11}^{E} & c_{12}^{E} & c_{13}^{E} & 0 & 0 & 0 \\ c_{12}^{E} & c_{11}^{E} & c_{23}^{E} & 0 & 0 & 0 \\ c_{13}^{E} & c_{13}^{E} & c_{33}^{E} & 0 & 0 & 0 \\ 0 & 0 & 0 & c_{44}^{E} & 0 & 0 \\ 0 & 0 & 0 & 0 & c_{44}^{E} & 0 \\ 0 & 0 & 0 & 0 & 0 & \frac{c_{11}^{E}-c_{12}^{E}}{2} \end{bmatrix} \quad (1)$$

$$\mathbf{e} = \begin{bmatrix} 0 & 0 & 0 & 0 & e_{15} & 0 \\ 0 & 0 & 0 & e_{15} & 0 & 0 \\ e_{31} & e_{31} & e_{33} & 0 & 0 & 0 \end{bmatrix} \quad (2)$$

and

$$\boldsymbol{\varepsilon}^{S} = \begin{bmatrix} \varepsilon_{11}^{S} & 0 & 0 \\ 0 & \varepsilon_{22}^{S} & 0 \\ 0 & 0 & \varepsilon_{33}^{S} \end{bmatrix} \quad (3)$$

respectively.

The TE, TSE, LTE, and RUS samples were cut from a large sample with a size of 40 × 40 × 5.0 mm, and the LE and RE samples were cut from two cylindrical samples with a diameter of 10 mm and a height of 10 mm. Samples were cut using a diamond wire cutting saw (Kejing STX-202AQ) and ground using an automatic grinding and polishing machine (Kejing UNIPOL-802). Their sizes were measured using a digital height gauge (Mikrometry DHG-050), as shown in Table II. The shadow surfaces of the ER samples, as shown in

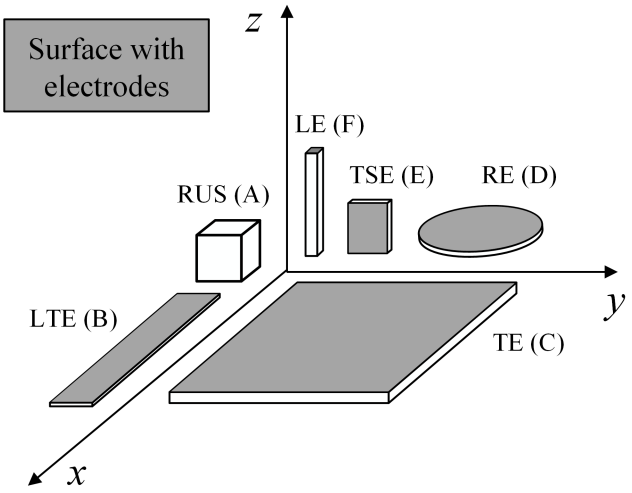

Fig. 1. Samples used in ER and RUS.

TABLE II
SIZES OF SAMPLES USED IN ER AND RUS

Sample	Resonator	Dimension (mm)	Constants
A	RUS	4.709 × 5.150 × 4.312	c_{ii}^{E}, e_{ij}
B	LTE	19.99 × 4.124 × 0.315	$s_{11}^{E}{}^{(a)}$, $k_{31}{}^{(a)}$, $d_{31}{}^{(a)}$
C	TE	20.00 × 20.00 × 1.167	c_{33}^{D}, c_{33}^{E}, k_t, e_{33}
D	RE	10.020 × 0.331	$s_{11}^{E}{}^{(b)}$, s_{12}^{E}, $k_{31}{}^{(b)}$, $d_{31}{}^{(b)}$
E	TSE	0.332 × 2.901 × 4.851	c_{55}^{D}, s_{55}^{E}, c_{55}^{E}, k_{15}, d_{15}
F	LE	1.798 × 1.052 × 10.018	s_{33}^{D}, s_{33}^{E}, k_{33}, d_{33}

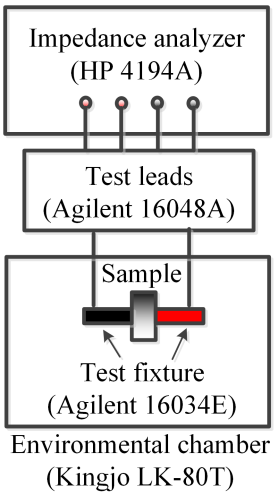

Fig. 2. Setup for measuring the TD of the capacitances and electric impedance curves of piezoelectric samples.

Fig. 1, were fully sputtered with gold electrodes using a Kejing VTC-16-D sputter. The thickness of the electrode surfaces was approximately 17 nm. Note that no electrode was sputtered on the surface of the RUS sample.

B. Measurement of Dielectric Constants and Electric Impedance Curves

The RUS sample was used to measure the free and clamped dielectric properties. The low-frequency capacitance C_L was measured at 5 kHz using an HP 4194A impedance analyzer and an HP 16034E impedance test fixture, as shown in Fig. 2. The HP 4194A impedance analyzer has the maximum upper working frequency of 15 MHz when an Agilent 16034E test fixture is connected to it using Agilent 16048A test leads. To ensure the measurement accuracy, the setup must be calibrated according to its manual after the configuration of the start and stop frequencies. The high-frequency capacitance C_H was measured at 30 MHz using an HP 4195A impedance analyzer and an HP 16194A impedance test fixture. To measure the TD of the capacitance, the fixture and sample were placed in a temperature chamber (Kingjo LK-80T) during the measurement. The free and clamped dielectric properties were then obtained using $\varepsilon^T = C_L t/A$ and $\varepsilon^S = C_H t/A$, respectively, where t is the thickness along the direction perpendicular to the electrode surface and A is the area of the sample's electrode surface. The dielectric constants ε_{11}^T, ε_{33}^T, ε_{11}^S, and ε_{33}^S, were determined using this method in this study.

The electric impedance curves were measured using the setup shown in Fig. 2. The fixture and the samples were placed in the temperature chamber. A control panel developed using LabVIEW was used to establish the sweeping frequency band and the number of sweeping points. The resonance and antiresonance frequencies of the different resonators can be obtained from their electric impedance curves. Typically, there are multiple resonance and antiresonance frequencies in the electric impedance curves. If not specified, the resonance and antiresonance frequencies used in the ER method are the fundamental ones.

C. ER Method

The ER method is described in detail in the IEEE Standard on piezoelectricity [2]. For ease of understanding, some important equations (4)–(18) in the standard are cited and listed here. The resonance frequencies (f_r) and antiresonance frequencies (f_a) of the TE, TSE, LE, and LTE resonators were measured using an HP 4194A impedance analyzer. From the TE resonator, c_{33}^D, k_t, c_{33}^E, and e_{33} can be calculated using

$$c_{33}^D = 4\rho l_z^2 f_a^2 \tag{4}$$

$$k_t^2 = \frac{\pi f_r}{2 f_a} \tan\left(\frac{\pi \Delta f}{2 f_a}\right) \tag{5}$$

$$c_{33}^E = c_{33}^D\left(1 - k_t^2\right) \tag{6}$$

and

$$e_{33} = k_t \sqrt{\varepsilon_{33}^S c_{33}^D} \tag{7}$$

respectively, where $\Delta f = f_a - f_r$. From the TSE resonator, c_{55}^D, k_{15}, s_{55}^E, and d_{15} can be calculated using

$$c_{55}^D = 4\rho l_x^2 f_a^2 \tag{8}$$

$$k_{15}^2 = \frac{\pi f_r}{2 f_a} \cot\left(\frac{\pi f_r}{2 f_a}\right) \tag{9}$$

$$s_{55}^E = \frac{1}{c_{55}^E} = \frac{1}{c_{55}^D\left(1 - k_{15}^2\right)} \tag{10}$$

and

$$d_{15} = k_{15}\sqrt{\varepsilon_{11}^{\mathrm{T}} s_{44}^{\mathrm{E}}} \tag{11}$$

respectively. From the LE resonator, s_{33}^{D}, k_{33}, s_{33}^{E}, and d_{33} can be calculated using

$$s_{33}^{\mathrm{D}} = \frac{1}{4\rho l_z^2 f_a^2} \tag{12}$$

$$k_{33}^2 = \frac{\pi f_r}{2 f_a} \tan\left(\frac{\pi \Delta f}{2 f_a}\right) \tag{13}$$

$$s_{33}^{\mathrm{E}} = \frac{s_{33}^{\mathrm{D}}}{1 - k_{33}^2} \tag{14}$$

and

$$d_{33} = k_{33}\sqrt{\varepsilon_{33}^{\mathrm{T}} s_{33}^{\mathrm{E}}} \tag{15}$$

respectively. From the LTE resonator, s_{11}^{E}, k_{31}, and d_{31} can be calculated using

$$s_{11}^{\mathrm{E}} = \frac{1}{4\rho {l_x}^2 f_r^2} \tag{16}$$

$$-\frac{k_{31}^2}{1 - k_{31}^2} = \frac{\pi f_a}{2 f_r} \cot\left(\frac{\pi f_a}{2 f_r}\right) \tag{17}$$

and

$$d_{31} = -\sqrt{k_{31}^2 \varepsilon_{33}^{\mathrm{T}} s_{11}^{\mathrm{E}}} \tag{18}$$

respectively. From the RE resonator, Poisson's ratio σ^{E} [29] can be calculated using

$$\frac{f_s^{(1)}}{f_s^{(0)}} = \frac{\eta_1}{\eta_0}\left[\frac{1 + \frac{1}{3}\left(\sigma^{\mathrm{E}}\right)^2 t^2 A_0(r, \eta_0)}{1 + \frac{1}{3}\left(\sigma^{\mathrm{E}}\right)^2 t^2 A_1(r, \eta_1)}\right]^{\frac{1}{2}} \tag{19}$$

where r and t are the radius and thickness of the RE resonator, respectively; $f_s^{(0)}$ and $f_s^{(1)}$ are the fundamental and first overtone resonance frequencies, respectively; and η_0 and η_1 are the two minimum positive roots of

$$\eta J_0(\eta) = \left(1 - \sigma^{\mathrm{E}}\right) J_1(\eta) \tag{20}$$

where J_0 and J_1 are the zero- and first-order Bessel functions of the first kind, respectively, and

$$A_0(r, \eta_0) = \frac{\left[\left(\eta_0^2 + 1\right) J_0^2(\eta_0) + \left(\eta_0^2 - 1\right) J_1^2(\eta_0) - 1\right]}{\eta_0^2\left[J_0^2(\eta_0) + J_1^2(\eta_0)\right] - 2\eta_0 J_0(\eta_0) J_1(\eta_0)} \times \frac{\eta_0^2}{r^2} \tag{21}$$

$$A_1(r, \eta_1) = \frac{\left[\left(\eta_1^2 + 1\right) J_0^2(\eta_1) + \left(\eta_1^2 - 1\right) J_1^2(\eta_1) - 1\right]}{\eta_1^2\left[J_0^2(\eta_1) + J_1^2(\eta_1)\right] - 2\eta_1 J_0(\eta_1) J_1(\eta_1)} \times \frac{\eta_1^2}{r^2}. \tag{22}$$

Furthermore, s_{11}^{E} and s_{12}^{E} can be calculated using

$$s_{11}^{\mathrm{E}} = \frac{\eta_1^2}{\rho \pi^2 (2r)^2 (f_r)^2\left[1 - \left(\sigma^{\mathrm{E}}\right)^2\right]} \tag{23}$$

and

$$s_{12}^{\mathrm{E}} = -\sigma^{\mathrm{E}} s_{11}^{\mathrm{E}} \tag{24}$$

respectively. In this study, the values of s_{11}^{E} were determined using (16) and (23) and are denoted as $s_{11}^{\mathrm{E}\,(\mathrm{a})}$ and $s_{11}^{\mathrm{E}\,(\mathrm{b})}$, respectively. The planar coupling factor k_p [30] and the transverse coupling factor k_{31} [2] can be calculated using (25), as shown at the bottom of the next page, and

$$k_{31}^2 = \left(\frac{1 - \sigma^{\mathrm{E}}}{2}\right) k_p^2 \tag{26}$$

respectively. The piezoelectric strain constants d_{31} can be calculated using

$$d_{31} = -k_p\sqrt{\varepsilon_{33}^{\mathrm{T}} s_{11}^{\mathrm{E}}\left(1 - \sigma^{\mathrm{E}}\right)/2}. \tag{27}$$

In this study, the values of k_{31} determined using (17) and (26) are denoted by $k_{31}^{(\mathrm{a})}$ and $k_{31}^{(\mathrm{b})}$, respectively. The values of d_{31} determined using (18) and (27) are denoted by $d_{31}^{(\mathrm{a})}$ and $d_{31}^{(\mathrm{b})}$, respectively. The elastic compliance constant s_{13}^{E} is the only parameter that cannot be obtained directly from the resonant mode in ER. It can be calculated using [31]

$$c_{13}^{\mathrm{E}} = \frac{e_{33} - d_{33} c_{33}^{\mathrm{E}}}{2 d_{31}} \tag{28}$$

$$e_{31} = \frac{\varepsilon_{33}^{\mathrm{T}} - \varepsilon_{33}^{S} - d_{33} e_{33}}{2 d_{31}} \tag{29}$$

and

$$s_{13}^{\mathrm{E}} = \frac{-c_{13}^{\mathrm{E}} s_{33}^{\mathrm{E}} d_{31}}{e_{31} - d_{33} c_{13}^{\mathrm{E}}}. \tag{30}$$

Sherrit et al. [14] presented an alternative method to determine s_{13}^{E}. Given an initial estimate of s_{13}^{E}, the value of c_{33}^{D} can be determined using

$$\mathbf{c}^{\mathrm{D}} = \left[\mathbf{s}^{\mathrm{D}}\right]^{-1} = \left[\mathbf{s}^{\mathrm{E}} - \mathbf{d}^{t}\left[\boldsymbol{\varepsilon}^{\mathrm{T}}\right]^{-1}\mathbf{d}\right]^{-1} \tag{31}$$

where the superscript "t" denotes the inversion. The value of s_{13}^{E} was then adjusted until the calculated value of c_{33}^{D} was equal to that determined from the TE resonator. In this study, the values of s_{13}^{E} determined using (30) and (31) are denoted as $s_{13}^{\mathrm{E}\,(\mathrm{a})}$ and $s_{13}^{\mathrm{E}\,(\mathrm{b})}$, respectively.

D. RUS Method

The principle of RUS [32] for PMs can be described as follows. The resonance frequencies of a piezoelectric sample can be determined by its geometrical sizes, density, and full tensorial material properties, that is, elastic, piezoelectric, and dielectric properties. Conversely, the full tensorial material properties of the sample can be determined from its resonance frequencies after its geometrical sizes and density are known. The RUS technique consists of two parts. One is the forward problem and the other is the backward problem.

The forward problem involves the derivation and numerical solution of the eigenvalue equation. The eigenvalue equation is often derived using the Rayleigh–Ritz method [33]. The Lagrangian for the vibration of the piezoelectric body under traction-free boundary conditions is given by

$$L = \frac{1}{2}\iiint\Big[S_{ij} c_{ijkl}^{\mathrm{E}} S_{kl} - \phi_{,m}\varepsilon_{mn}^{S}\phi_{,n} + 2\phi_{,m} e_{mkl} S_{kl} - \rho\omega^2 u_i u_i\Big] dV \tag{32}$$

where c_{ijkl}^{E}, ε_{mn}^{S}, and e_{mkl} are the elastic stiffness constant under a constant electric field, clamped dielectric constant, and piezoelectric stress constant, respectively; S_{ij}, u_i, and ϕ are the strain component, displacement component, and electric potential, respectively; and ρ and ω are the density and angular frequency, respectively. u_i and ϕ can be approximately formulated by the sum of the linear combination of orthogonal basis functions, i.e.,

$$u_i = \sum_{p=1}^{N} a_p^{(i)} v_p \tag{33}$$

and

$$\phi = \sum_{r=1}^{M} b_r \psi_r \tag{34}$$

where $\{v_p\}$ and $\{\psi_r\}$ are orthogonal basis functions, such as Legendre functions, and $\{a_p^{(i)}\}$ and $\{b_r\}$ are coefficients. Substituting (33) and (34) into (32) and using

$$\frac{\partial L}{\partial a_{\mathrm{p}}^{(\mathrm{i})}} = 0, \quad \frac{\partial L}{\partial b_p} = 0 \tag{35}$$

we obtain

$$\left(\Gamma + \mathbf{\Omega}\mathbf{\Lambda}^{-1}\mathbf{\Omega}^{\mathrm{T}}\right)\mathbf{A} = \rho\omega^2\mathbf{A} \tag{36}$$

and

$$\mathbf{B} = \mathbf{\Lambda}^{-1}\mathbf{\Omega}^{\mathrm{T}}\mathbf{A} \tag{37}$$

where A and B are coefficient matrices, i.e.,

$$\mathbf{A} = \left[a_1^{(1)}, a_2^{(1)}, \ldots, a_N^{(1)}, a_1^{(2)}, a_2^{(2)}, \ldots, a_N^{(2)}, a_1^{(3)}, a_2^{(3)}, \ldots, a_N^{(3)}\right] \tag{38}$$

$$\mathbf{B} = [b_1, b_2, \ldots, b_{\mathrm{M}}] \tag{39}$$

where Γ, Ω, and Λ are the $3N \times 3N$, $3N \times M$, and $M \times M$ matrices, respectively. Solving the eigenvalue equation, i.e., (36), we can obtain the resonance frequencies of the piezoelectric sample using the given geometrical sizes and material properties.

The backward problem is to determine the material properties based on the resonance frequencies. This procedure is used to identify the local minimum value of

$$F = \frac{1}{2}\sum_{i=1}^{K} w_i \left[f_{cal}^{(i)} - f_{\mathrm{meas}}^{(i)}\right]^2 \tag{40}$$

where $f_{\mathrm{meas}}^{(i)}$ is the ith measured resonance frequency, $f_{cal}^{(i)}$ is the ith resonance frequency calculated from the eigenvalue equation, and w_{i} is the weighting factor. The backward problem can be solved using nonlinear least-squares (NLS) methods such as the Gauss–Newton [34] and Levenberg–Marquardt (LM) [35] methods, or deep learning (DL) [36]. In this study, the LM method was used to solve the backward problem as it is flexible, controllable, stable, and reliable [32].

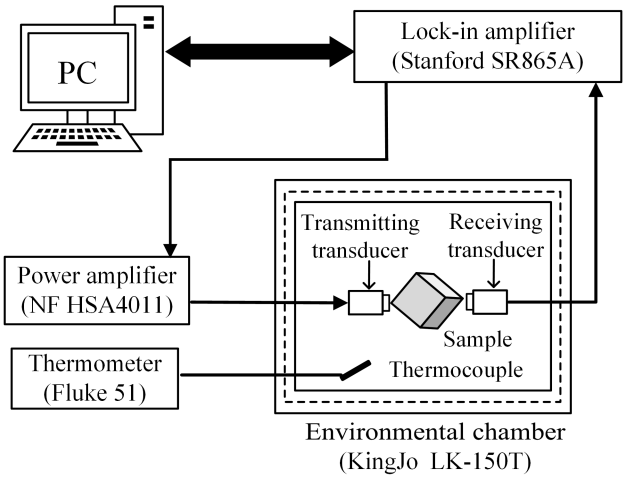

Fig. 3. RUS setup.

MINPACK [37] was used in our computation codes, which is a numerical subroutine library for function minimization and least-squares solutions based on the LM algorithm. Fig. 3 shows the RUS setup. A personal computer was connected to a Stanford SR865A lock-in amplifier. An RUS control panel was developed using LabVIEW. The sweeping frequency band (150–800 kHz), total sweeping time (300 s), and the signal duration at each frequency point (16 ms) were set by the control panel. The frequency-sweeping signal was generated by the lock-in amplifier and subsequently amplified by an NF HSA4011 power amplifier. Two ultrasonic transducers, fabricated using $PbNb_2O_6$ ceramics, were used to excite and receive the sample vibration. $PbNb_2O_6$ ceramics were often used to fabricate high-temperature transducers because of their high-Curie temperature of 570 °C. One transducer was driven by the amplified signal. The vibration of the piezoelectric sample was excited and sensed by another transducer. The electrical signals were output from the receiving transducer and input to the lock-in amplifier. After the lock-in amplification, the resonance spectrum of the sample was generated.

To measure the TD of the resonant ultrasound spectra, the transmitting and receiving transducers and the sample were placed in the temperature chamber (Kingjo LK-80T).

III. Results and Discussion

A. Resonant Ultrasound Spectra and Identified Resonance Frequencies

Fig. 4 shows the resonant ultrasound spectra of sample A in Table II from 150 to 500 kHz at 20 °C and 100 °C. Each peak in Fig. 4 represents a resonance mode. The values of f_{meas} in Tables III and IV are the resonance frequencies at 20 °C and 100 °C, respectively. Most of the resonance frequencies increase with temperature. Mode identification is the most difficult step in the RUS procedure because modes omission and modes overlap cannot be avoided during the measurement of resonant ultrasound spectra. Prior information of EPCs $\{c_{11}^{\mathrm{E}}$,

$$\frac{k_p^2}{1-k_p^2} = \frac{\left(1-\sigma^{\mathrm{E}}\right)J_1\left[\eta_1(1+\Delta f/f_r)\right] - \eta_1(1+\Delta f/f_r)J_0\left[\eta_1(1+\Delta f/f_r)\right]}{\left(1+\sigma^{\mathrm{E}}\right)J_1\left[\eta_1(1+\Delta f/f_r)\right]} \tag{25}$$

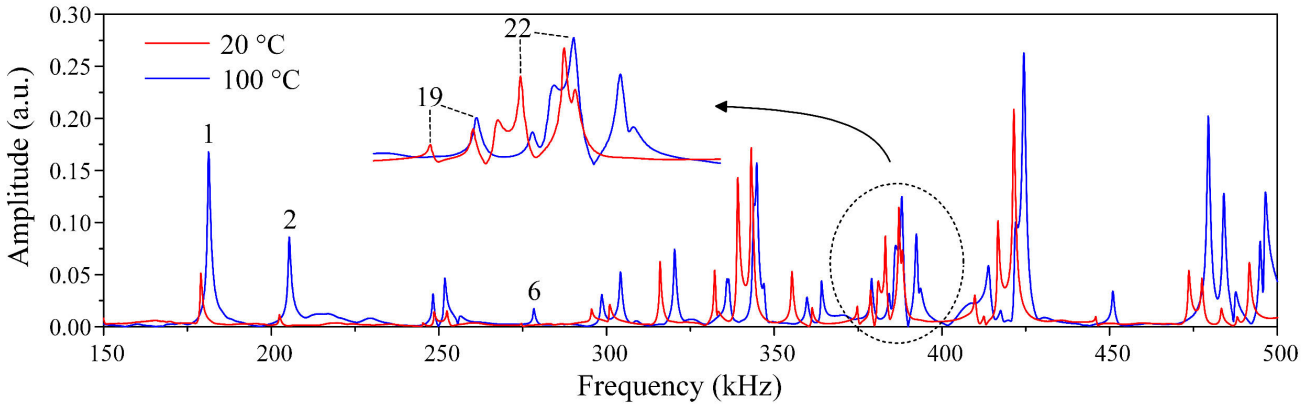

Fig. 4. Resonant ultrasound spectra from 150 to 500 kHz at 20 °C and 100 °C.

TABLE III
MEASURED FREQUENCIES f_{MEAS} (UNIT: KHZ) AND CALCULATED RESONANCE FREQUENCIES f_{cal} (UNIT: KHZ) USING THE CONSTANTS DETERMINED BY RUS AT 20 °C

	f_{meas}	f_{cal}	Diff [a]		f_{meas}	f_{cal}	Diff		f_{meas}	f_{cal}	Diff		f_{meas}	f_{cal}	Diff
1	—	—	—	27	417.05	418.04	0.24	53	591.72	590.27	0.25	79	685.78	687.04	0.18
2	202.14	202.32	0.09	28	421.07	420.33	0.18	54	593.16	594.05	0.15	80	688.15	688.90	0.11
3	245.60	245.03	0.23	29	446.12	446.70	0.13	55	595.19	594.95	0.04	81	688.87	689.75	0.13
4	248.56	249.05	0.20	30	473.92	474.43	0.11	56	—	—	—	82	690.98	690.23	0.11
5	252.96	252.92	0.02	31	477.31	477.57	0.05	57	—	—	—	83	701.65	700.52	0.16
6	274.97	274.89	0.03	32	483.31	483.23	0.02	58	—	—	—	84	708.42	709.13	0.10
7	284.07	284.72	0.23	33	488.27	487.50	0.16	59	611.31	611.14	0.03	85	—	—	—
8	—	—	—	34	491.61	491.99	0.08	60	618.97	619.63	0.11	86	711.38	712.35	0.14
9	295.49	296.16	0.23	35	502.65	502.00	0.13	61	622.73	623.70	0.16	87	714.26	714.41	0.02
10	300.52	300.03	0.16	36	503.54	502.55	0.20	62	—	—	—	88	715.99	716.37	0.05
11	315.88	315.97	0.03	37	506.46	506.52	0.01	63	628.62	628.55	0.01	89	721.79	722.56	0.11
12	332.01	332.18	0.05	38	508.96	509.19	0.05	64	630.65	631.67	0.16	90	—	—	—
13	333.02	333.51	0.15	39	511.62	511.82	0.04	65	636.40	637.26	0.13	91	724.83	724.41	0.06
14	338.82	338.29	0.16	40	513.23	513.41	0.03	66	643.89	642.66	0.19	92	728.77	729.20	0.06
15	342.88	342.43	0.13	41	515.64	515.74	0.02	67	—	—	—	93	—	—	—
16	343.68	343.85	0.05	42	522.75	521.94	0.16	68	655.61	654.26	0.21	94	732.66	732.41	0.03
17	—	—	—	43	524.95	524.47	0.09	69	657.30	657.37	0.01	95	736.85	735.59	0.17
18	361.37	361.61	0.07	44	533.54	533.48	0.01	70	662.30	661.88	0.06	96	743.83	744.02	0.03
19	374.74	374.68	0.02	45	542.34	541.39	0.18	71	665.17	664.29	0.13	97	748.28	748.07	0.03
20	378.46	378.27	0.05	46	547.29	547.98	0.13	72	—	—	—	98	750.48	751.00	0.07
21	380.79	379.91	0.23	47	553.64	553.97	0.06	73	667.12	668.10	0.15	99	756.61	757.04	0.06
22	382.70	382.65	0.01	48	557.91	557.35	0.10	74	671.06	671.49	0.06	100	757.92	758.80	0.12
23	—	—	—	49	570.14	569.15	0.17	75	673.09	673.30	0.03	101	766.30	767.28	0.13
24	—	—	—	50	574.08	574.38	0.05	76	677.99	677.57	0.06				
25	410.33	410.89	0.14	51	575.56	575.71	0.03	77	683.62	683.71	0.01				
26	413.12	414.00	0.21	52	580.59	580.88	0.05	78	—	—	—				

[a] $\text{diff} = \left|\frac{f_{meas} - f_{cal}}{(f_{meas} + f_{cal})/2}\right| \times 100$

c_{12}^{E}, c_{13}^{E}, c_{33}^{E}, c_{44}^{E}, e_{15}, e_{31}, $e_{33}\}$ is needed to perform mode identification; some of this information can be obtained using the UPE and ER methods. Note that some resonance modes may occur in the spectrum measured at temperature T_1 but disappear when measured at T_2. The resonance frequencies corresponding to these modes can be obtained by fitting the TD of these resonance frequencies with polynomial functions using the measured resonance frequencies at some temperature points. For example, the resonance frequencies corresponding to modes 53, 68, and 89 at 100 °C were obtained using this method, as shown in Table IV.

B. Results Characterized Using ER and RUS

Notably, all measurements in this study were conducted every 10 °C from 20 °C to 110 °C. Therefore, the material constants of the piezoelectric samples were determined within

TABLE IV
MEASURED FREQUENCIES f_{meas} (UNIT: KHZ) AND CALCULATED RESONANCE FREQUENCIES f_{cal} (UNIT: KHZ) USING THE CONSTANTS DETERMINED BY RUS AT 100 °C

	f_{meas}	f_{cal}	Diff [a]		f_{meas}	f_{cal}	Diff		f_{meas}	f_{cal}	Diff		f_{meas}	f_{cal}	Diff
1	—	—	—	27	421.45	422.12	0.16	53	597.16	596.09	0.18	79	692.63	692.96	0.05
2	205.69	205.54	0.07	28	424.25	422.44	0.43	54	598.53	599.30	0.13	80	695.51	695.90	0.06
3	248.22	247.09	0.46	29	451.28	450.96	0.07	55	602.30	599.99	0.38	81	697.33	696.31	0.15
4	252.03	251.92	0.04	30	479.08	479.30	0.05	56	—	—	—	82	698.56	697.88	0.10
5	255.8	255.33	0.18	31	484.46	483.91	0.11	57	—	—	—	83	710.49	708.17	0.33
6	278.65	278.37	0.10	32	487.33	485.89	0.30	58	—	—	—	84	715.78	715.39	0.06
7	287.15	287.39	0.08	33	494.95	493.30	0.33	59	618.63	617.28	0.22	85	—	—	—
8	—	—	—	34	496.60	496.32	0.06	60	625.82	625.54	0.04	86	718.95	718.55	0.05
9	298.83	298.47	0.12	35	507.14	505.31	0.36	61	631.11	631.45	0.05	87	722.25	721.30	0.13
10	304.25	302.74	0.50	36	509.38	507.45	0.38	62	—	—	—	88	725.13	724.91	0.03
11	320.5	320.34	0.05	37	512.89	512.21	0.13	63	637.29	636.37	0.15	89	730.56	731.01	0.06
12	336.11	335.82	0.09	38	516.11	515.73	0.07	64	638.81	638.18	0.10	90	—	—	—
13	336.53	336.36	0.05	39	517.29	516.06	0.24	65	642.37	642.28	0.01	91	733.64	733.51	0.02
14	343.9	342.57	0.39	40	518.27	517.52	0.14	66	652.40	649.98	0.37	92	735.62	735.11	0.07
15	344.57	343.82	0.22	41	521.65	520.99	0.13	67	—	—	—	93	—	—	—
16	347.12	346.44	0.20	42	529.39	527.76	0.31	68	663.76	660.91	0.43	94	739.77	738.94	0.11
17	—	—	—	43	531.09	529.43	0.31	69	664.20	663.25	0.14	95	744.85	742.31	0.34
18	364.16	363.30	0.24	44	538.15	538.15	0.00	70	669.41	668.48	0.14	96	752.51	751.51	0.13
19	378.68	378.43	0.07	45	548.90	547.00	0.35	71	671.48	668.97	0.38	97	755.09	753.68	0.19
20	384.8	384.03	0.20	46	553.30	553.31	0.00	72	—	—	—	98	758.22	757.93	0.04
21	385.95	384.41	0.40	47	558.55	557.46	0.19	73	674.40	674.51	0.02	99	764.35	763.69	0.09
22	387.94	387.31	0.16	48	563.88	562.96	0.16	74	678.16	676.98	0.17	100	766.51	766.13	0.05
23	—	—	—	49	576.28	574.79	0.26	75	681.97	681.29	0.10	101	775.19	773.42	0.23
24	—	—	—	50	580.63	580.56	0.01	76	684.34	682.61	0.25				
25	413.96	413.56	0.10	51	582.92	581.34	0.27	77	689.67	688.82	0.12				
26	417.35	418.00	0.16	52	587.02	586.60	0.07	78	—	—	—				

[a] $\text{diff} = \left|\frac{f_{meas} - f_{cal}}{(f_{meas} + f_{cal})/2}\right| \times 100$

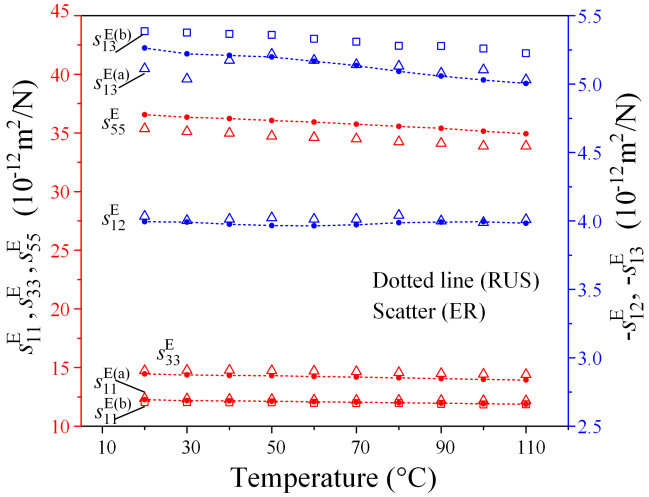

Fig. 5. TD of elastic compliance constants $\{s_{11}^E, s_{12}^E, s_{13}^E, s_{33}^E, s_{44}^E\}$, where scatter and dotted lines are the results characterized using ER and RUS, respectively.

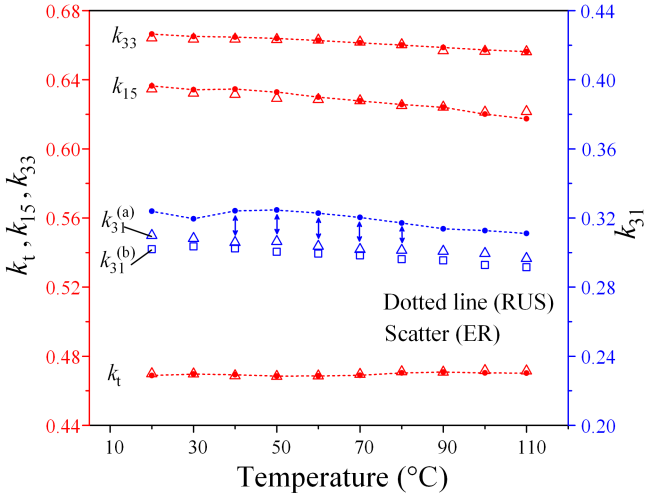

Fig. 6. TD of electromechanical coupling constants $\{k_{15}, k_{31}, k_{33}, k_t\}$, where scatter and dotted lines are the results characterized using ER and RUS, respectively. Data with a relative error greater than 5% are marked using double-headed arrows.

the same temperature range with the same interval using RUS and ER.

Figs. 5–7 show the TD of the elastic compliance constants $\{s_{11}^E, s_{12}^E, s_{13}^E, s_{33}^E, s_{44}^E\}$, electromechanical coupling constants $\{k_{15}, k_{31}, k_{33}, k_t\}$, and piezoelectric strain constants $\{d_{15}, d_{31}, d_{33}\}$, respectively, where the scatter and dotted lines are the results determined using ER and RUS, respectively. The

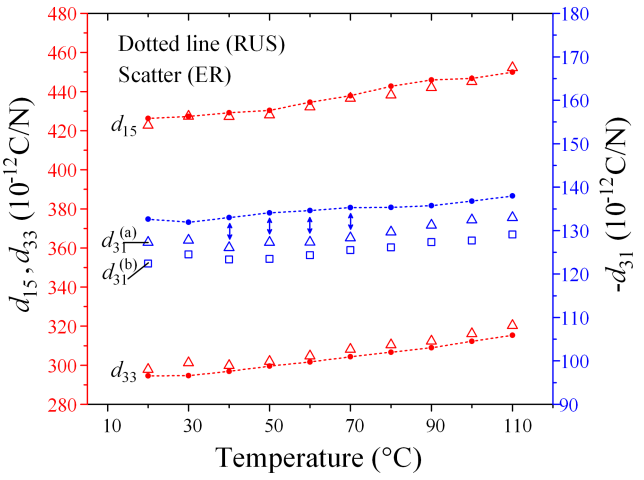

Fig. 7. TD of piezoelectric strain constants $\{d_{15}, d_{31}, d_{33}\}$, where points and dotted lines are the results characterized using ER and RUS, respectively. Data with a relative error greater than 5% are marked using double-headed arrows.

values of s_{11}^{E} determined from the RE resonator agree well with those determined using RUS from 20 °C to 110 °C, as shown in Fig. 5. The relative errors are less than 1.8% in this temperature range. The relative errors between the values of s_{11}^{E} determined from the LTE resonator and those determined using RUS were less than 2.3%. The values of s_{12}^{E} determined using ER agree very well with those determined using RUS from 20 °C to 110 °C. The relative errors are less than 1.5% over the entire temperature range. The values of s_{33}^{E} determined using ER are higher than those determined using RUS from 20 °C to 110 °C. The relative errors are less than 3.4% over the entire temperature range. The values of s_{55}^{E} determined using RUS were higher than those determined using ER from 20 °C to 110 °C. The relative errors are greater than 3.0% over the entire temperature range. The maximal relative error occurs at 80 °C, which is approximately 3.8%. The values of $s_{13}^{\mathrm{E}\,(\mathrm{a})}$ determined using (30) agree well with those determined using RUS from 40 °C to 110 °C. However, the values of $s_{13}^{\mathrm{E}\,(\mathrm{b})}$ determined using (31) are higher than those determined using RUS from 20 °C to 110 °C. The relative errors are greater than 2.3% over the entire temperature range. The maximum relative error occurs at 100 °C, which is equivalent to 4.4%. The values of s_{13}^{E} determined using (31) are higher than those determined using (30). The maximum relative error occurs at 30 °C, which is equivalent to 6.3%. The TD of $\{k_{15}, k_{33}, k_t\}$ determined using ER agrees very well with that determined using RUS, as shown in Fig. 6. The relative errors between the values of k_{15} determined using ER and those determined using RUS are less than 0.6%, and those corresponding to k_{33} and k_t are less than 0.4% and 0.3%, respectively, from 20 °C to 110 °C. The values of k_{31} determined using RUS are higher than those determined from the LTE resonator using ER from 20 °C to 110 °C. The relative errors are greater than 3.6% over the entire temperature range. The maximum relative error occurs at 60 °C, which is approximately equivalent to 6.1%. Moreover, the relative errors between the values of k_{31} determined from the LTE and RE resonators using ER are less than 2.6% from 20 °C to 110 °C. The TD of d_{15} determined using ER agrees well with that determined using RUS, as shown in Fig. 7. The relative errors between the values of d_{15} determined using ER and those determined using RUS are less than 1.1% from 20 °C to 110 °C. The relative errors between the values of d_{33} determined using ER and those determined using RUS are less than 2.3% from 20 °C to 110 °C. However, the relative errors between the values of d_{31} determined from the LTE resonator using ER and those determined using RUS are greater than 3.2% from 20 °C to 110 °C. The maximal relative error occurs at 60 °C, which is approximately equivalent to 5.5%. Moreover, the absolute values of d_{31} determined using RUS are greater than those determined using ER over the entire temperature range. Note that the relative errors between the values of d_{31} determined from the LTE and RE resonators using ER are greater than 2.2% from 20 °C to 110 °C. The maximal relative error is at 20 °C, which is approximately equivalent to 3.9%.

In the ER method, the electromechanical coupling factors $\{k_t, k_{15}, k_{33}, k_{31}\}$ are calculated using (5), (9), (13), and (17), respectively. Assuming that $\{k_t, k_{15}, k_{33}, k_{31}\}$ are just functions of the antiresonant frequency f_a, we have

$$\frac{\Delta k_{15}}{k_{15}} = \frac{1}{2}\left[\frac{\frac{\pi f_r}{2f_a}}{\sin\left(\frac{\pi f_r}{2f_a}\right)\cos\left(\frac{\pi f_r}{2f_a}\right)} - 1\right]\frac{\Delta f_a}{f_a} \tag{41}$$

$$\frac{\Delta k_t}{k_t} = \frac{1}{2}\left[\frac{\frac{\pi f_r}{2f_a}}{\sin\left(\frac{\pi (f_a - f_r)}{2f_a}\right)\cos\left(\frac{\pi (f_a - f_r)}{2f_a}\right)} - 1\right]\frac{\Delta f_a}{f_a} \tag{42}$$

$$\frac{\Delta k_{33}}{k_{33}} = \frac{1}{2}\left[\frac{\frac{\pi f_r}{2f_a}}{\sin\left(\frac{\pi (f_a - f_r)}{2f_a}\right)\cos\left(\frac{\pi (f_a - f_r)}{2f_a}\right)} - 1\right]\frac{\Delta f_a}{f_a} \tag{43}$$

$$\frac{\Delta k_{31}}{k_{31}} = \frac{1}{2 - \pi\frac{f_a}{f_r}\cot\left(\frac{\pi f_a}{2f_r}\right)}\left[1 - \frac{\frac{\pi f_a}{2f_r}}{\sin\left(\frac{\pi f_a}{2f_r}\right)\cos\left(\frac{\pi f_a}{2f_r}\right)}\right]\frac{\Delta f_a}{f_a}. \tag{44}$$

The resonant and antiresonant frequencies $\{f_r, f_a\}$ corresponding to the TSE, TE, LE, and LTE resonators used in this study at 20 °C are {2995.00 kHz, 3720.00 kHz}, {1792.00 kHz, 1987.00 kHz}, {153.625 kHz, 196.750 kHz}, and {80.765 kHz, 84.060 kHz}, respectively. If the measurement error of f_a is 1%, the errors will be 1.7% for k_{15}, 4.2% for k_t, 1.4% for k_{33}, and 12% for k_{31}.

In ER, d_{31} is calculated using (18). e_{31} can be calculated using

$$e_{31} = d_{31}\left(c_{11}^{\mathrm{E}} + c_{12}^{\mathrm{E}}\right) + d_{33}c_{13}^{\mathrm{E}}. \tag{45}$$

The error of k_{31} propagates to d_{31}. Furthermore, the errors of $\{d_{31}, d_{33}, c_{11}^{\mathrm{E}}, c_{12}^{\mathrm{E}}, c_{13}^{\mathrm{E}}\}$ are passed to e_{31}. Therefore, the accuracy of the values of d_{31} and e_{31} characterized using ER may be low due to the large error of k_{31}.

Table V lists the values of the elastic stiffness constants $\{c_{11}^{\mathrm{E}}, c_{12}^{\mathrm{E}}, c_{13}^{\mathrm{E}}, c_{33}^{\mathrm{E}}, c_{44}^{\mathrm{E}}\}$ characterized using RUS and those calculated from the ER results. The values of $\{c_{11}^{\mathrm{E}}, c_{12}^{\mathrm{E}}, c_{13}^{\mathrm{E}}, c_{33}^{\mathrm{E}}\}$ characterized using RUS agree well with those calculated from the ER results. However, the relative error between the

TABLE V
ELASTIC STIFFNESS CONSTANTS $\{c_{11}^{E}, c_{12}^{E}, c_{13}^{E}, c_{33}^{E}, c_{44}^{E}\}$ (UNIT: 10^{10}N/M^2) CHARACTERIZED USING RUS AND ER

T (°C)	c_{11}^{E}			c_{12}^{E}			c_{13}^{E}			c_{33}^{E}			c_{44}^{E}		
	RUS	ER	Diff[a]	RUS	ER	Diff	RUS	ER	Diff	RUS	ER	Diff	RUS	ER	Diff
20	14.37	14.42	0.34	8.220	8.325	1.3	8.231	8.312	0.98	12.92	13.09	1.3	2.735	2.828	3.3
30	14.46	14.41	0.35	8.279	8.284	0.06	8.264	8.257	0.09	12.97	13.04	0.52	2.753	2.848	3.5
40	14.48	14.48	0.04	8.277	8.347	0.84	8.273	8.290	0.21	13.00	13.10	0.82	2.761	2.858	3.5
50	14.53	14.57	0.29	8.310	8.430	1.4	8.298	8.365	0.80	13.02	13.16	1.1	2.773	2.879	3.8
60	14.56	14.56	0.05	8.330	8.400	0.84	8.303	8.326	0.27	13.04	13.19	1.1	2.783	2.889	3.7
70	14.60	14.56	0.32	8.358	8.395	0.44	8.311	8.316	0.06	13.06	13.19	0.96	2.798	2.899	3.6
80	14.65	14.59	0.39	8.396	8.441	0.53	8.312	8.346	0.41	13.08	13.19	0.83	2.812	2.921	3.8
90	14.70	14.57	0.93	8.430	8.393	0.44	8.322	8.366	0.53	13.10	13.22	0.87	2.825	2.931	3.7
100	14.76	14.55	1.43	8.471	8.363	1.3	8.349	8.341	0.10	13.15	13.22	0.56	2.846	2.952	3.7
110	14.78	14.58	1.38	8.473	8.388	1.0	8.351	8.327	0.28	13.18	13.26	0.63	2.863	2.952	3.1

[a] $\text{Diff} = \left| \frac{c_{ij}^{E(\text{RUS})} - c_{ij}^{E(\text{ER})}}{\left(c_{ij}^{E(\text{RUS})} + c_{ij}^{E(\text{ER})}\right)/2} \right| \times 100$

TABLE VI
PIEZOELECTRIC STRESS CONSTANTS $\{e_{15,}-e_{31,}e_{33}\}$ (UNIT: C/M) CHARACTERIZED USING RUS AND ER

T (°C)	e_{15}			-e_{31}			e_{33}		
	RUS	ER	Diff[a]	RUS	ER	Diff	RUS	ER	Diff
20	11.66	11.96	2.5	5.72	6.03	5.3	16.22	16.37	0.93
30	11.76	12.18	3.5	5.65	6.49	13.9	16.41	16.46	0.27
40	11.85	12.21	3.0	5.70	5.36	6.1	16.58	16.62	0.27
50	11.93	12.33	3.2	5.76	5.13	11.6	16.76	16.84	0.50
60	12.10	12.49	3.2	5.77	5.12	11.8	17.00	17.09	0.57
70	12.25	12.66	3.3	5.77	5.20	10.3	17.27	17.39	0.66
80	12.45	12.80	2.8	5.71	5.13	10.6	17.60	17.71	0.60
90	12.60	12.96	2.8	5.68	5.40	5.1	17.89	17.97	0.45
100	12.71	13.14	3.3	5.70	5.20	9.2	18.21	18.33	0.65
110	12.88	13.35	3.6	5.75	5.34	7.3	18.50	18.62	0.65

[a] $\text{Diff} = \left| \frac{e_{ij}^{(\text{RUS})} - e_{ij}^{(\text{ER})}}{\left(e_{ij}^{(\text{RUS})} + e_{ij}^{(\text{ER})}\right)/2} \right| \times 100$

values of c_{44}^{E} characterized using RUS and ER is greater than 3% from 20 °C to 110 °C, which reaches 3.8% at 50 °C and 80 °C. c_{44}^{E} can be precisely characterized using RUS because the resonance frequencies are sensitive to its variations [38]. The large relative error between the values of c_{44}^{E} characterized using RUS and ER indicate that the values of c_{44}^{E} characterized using the former are more precise than those characterized using the latter.

Table VI lists the values of the piezoelectric stress constants $\{e_{15,}-e_{31,}e_{33}\}$ characterized using RUS and those calculated from the ER results. The relative error between the values of e_{33} characterized using RUS and ER is less than 1% from 20 °C to 110 °C, which indicates that the values of e_{33} characterized using RUS and ER agree very well. The relative error between the values of e_{15} characterized using RUS and ER is less than 3.6% from 20 °C to 110 °C. Note that the relative error between the values of e_{31} characterized using RUS and ER is large from 20 °C to 110 °C and reaches 13.9% at 30 °C.

Compared with $\{c_{11}^{E}, c_{12}^{E}, c_{13}^{E}, c_{33}^{E}, c_{44}^{E}, e_{15}, e_{33}\}$, most resonance frequencies are less sensitive to e_{31} [38], which means that the value of e_{31} determined using RUS may be less accurate than the values of $\{c_{11}^{E}, c_{12}^{E}, c_{13}^{E}, c_{33}^{E}, c_{44}^{E}, e_{15}, e_{33}\}$ determined using RUS. In RUS, the directly determined material constants from inversion are $[c^{E}]$ and $[e]$. $[s^{E}]$ is the inversion of $[c^{E}]$. d_{31} can then be calculated using

$$d_{31} = 2e_{31}s_{11}^{E} + e_{33}s_{13}^{E} \tag{46}$$

and k_{31} can be calculated using (18). The error of e_{31} is passed to d_{31} and k_{31}. Therefore, the large error in e_{31} may lead to large errors in d_{31} and k_{31}.

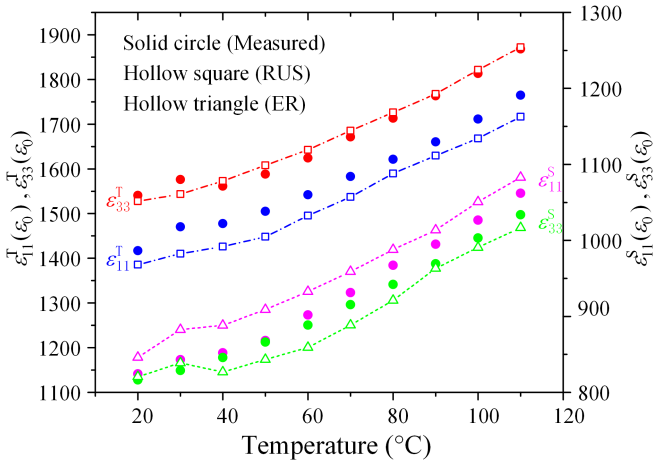

Fig. 8. TD of free and dielectric constants.

In summary, the results of k_{31}, d_{31}, and e_{31} may have large errors whether they are characterized using ER or RUS. This explains the large relative errors between the RUS and ER results, corresponding to k_{31}, d_{31}, and e_{31}. It is challenging to improve the characterization accuracies of k_{31}, d_{31}, and e_{31}.

C. TD of Dielectric Constants

During the RUS inversion, the measured clamped dielectric constants were used. Based on the results obtained using RUS, the free dielectric constants $\varepsilon_{11}^{\mathrm{T(c)}}$ and $\varepsilon_{33}^{\mathrm{T(c)}}$ can be calculated using

$$\varepsilon_{11}^{\mathrm{T(c)}} = \varepsilon_{11}^{\mathrm{S(m)}} + e_{15}^2 s_{55}^{\mathrm{E}} \tag{47}$$

and

$$\varepsilon_{33}^{\mathrm{T(c)}} = \varepsilon_{33}^{\mathrm{S(m)}} + 2e_{31}^2\left(s_{11}^{\mathrm{E}} + s_{12}^{\mathrm{E}}\right) + 4e_{31}e_{33}s_{13}^{\mathrm{E}} + e_{33}^2 s_{33}^{\mathrm{E}} \tag{48}$$

respectively, where $\varepsilon_{11}^{\mathrm{S(m)}}$ and $\varepsilon_{33}^{\mathrm{S(m)}}$ are the measured clamped dielectric constants using the method described in Section II-B, $\{e_{15},\ e_{31},\ e_{33}\}$ are the piezoelectric constants determined using RUS, as shown in Table VI, and $\{s_{11}^{\mathrm{E}}, s_{12}^{\mathrm{E}}, s_{13}^{\mathrm{E}}, s_{33}^{\mathrm{E}}, s_{55}^{\mathrm{E}}\}$ are the elastic compliance constants calculated from the elastic stiffness constants determined using RUS, as shown in Table V.

In the ER method, the measured free dielectric constants were used to calculate the remaining constants. Based on the results determined using ER, the clamped dielectric constants $\varepsilon_{11}^{\mathrm{S(c)}}$ and $\varepsilon_{33}^{\mathrm{S(c)}}$ can be determined using

$$\varepsilon_{11}^{\mathrm{S(c)}} = \varepsilon_{11}^{\mathrm{T(m)}} - d_{15}^2/s_{55}^{\mathrm{E}} \tag{49}$$

and

$$\varepsilon_{33}^{\mathrm{S(c)}} = \varepsilon_{33}^{\mathrm{T(m)}} - \left[2d_{31}^2\left(c_{11}^{\mathrm{E}} + c_{12}^{\mathrm{E}}\right) + 4d_{31}d_{33}c_{13}^{\mathrm{E}} + d_{33}^2 c_{33}^{\mathrm{E}}\right] \tag{50}$$

respectively, where $\varepsilon_{11}^{\mathrm{T(m)}}$ and $\varepsilon_{33}^{T(m)}$ are the measured free dielectric constants using the method described in Section II-B, $\{d_{15},\ d_{31},\ d_{33}\}$ are the piezoelectric constants determined using ER, as shown in Fig. 7, and $\{c_{11}^{\mathrm{E}}, c_{12}^{\mathrm{E}}, c_{13}^{\mathrm{E}}, c_{33}^{\mathrm{E}}, c_{55}^{\mathrm{E}}\}$ are the elastic stiffness constants calculated from the elastic compliance constants determined using ER, as shown in Fig. 5.

The blue, red, violet, and green circles in Fig. 8 represent the measured values of $\varepsilon_{11}^{\mathrm{T}}$, $\varepsilon_{33}^{\mathrm{T}}$, $\varepsilon_{11}^{\mathrm{S}}$, and $\varepsilon_{33}^{\mathrm{S}}$, respectively.

TABLE VII
ELASTIC CONSTANTS $\{c_{11}^{\mathrm{E}}, c_{12}^{\mathrm{E}}, c_{44}^{\mathrm{E}}, c_{33}^{\mathrm{D}}, c_{55}^{\mathrm{D}}\}$ (UNIT: 10 N/M2) DETERMINED USING UPE, RUS, AND ER

	UPE	RUS	Relative error (UPE, RUS)	ER	Relative error (UPE, ER)
c_{11}^{E}	14.31	14.37	0.42%	14.42	0.77%
c_{12}^{E}	8.191	8.220	0.35%	8.325	1.6%
c_{44}^{E}	2.755	2.735	0.72%	2.828	2.6%
c_{33}^{D}	16.81	16.56	1.5%	16.79	0.12%
c_{55}^{D}	4.588	4.598	0.22%	4.735	3.2%

The blue- and red-dotted lines with hollow squares are the calculated $\varepsilon_{11}^{\mathrm{T}}$ and $\varepsilon_{33}^{\mathrm{T}}$ values using (47) and (48), respectively, using the RUS results. The violet- and green-dotted lines with hollow triangles are calculated $\varepsilon_{11}^{\mathrm{S}}$ and $\varepsilon_{33}^{\mathrm{S}}$ from (49) and (50), respectively, using the ER results. All dielectric constants increase with an increase in temperature from 20 °C to 110 °C, as shown in Fig. 8. In the temperature range of 20 °C–110 °C, the maximum relative error between the value of $\varepsilon_{11}^{\mathrm{T}}$ measured and that calculated from (47) using the RUS results is 4.2% and that corresponding to $\varepsilon_{33}^{\mathrm{T}}$ is 2.1%. The maximum relative error between the value of $\varepsilon_{11}^{\mathrm{S}}$ measured and that calculated using (49) using the ER results is 4.6% and that corresponding to $\varepsilon_{33}^{\mathrm{S}}$ is 3.4%.

D. Additional Evaluation of the Results Characterized Using ER and RUS

RUS determines the material constants by inversion using NLS or DL. It is difficult to perform an error analysis of the results directly. However, the results obtained using RUS can be evaluated indirectly. The values of f_{cal} in Tables III and IV are the resonance frequencies calculated using the EPCs determined by RUS, as listed in Tables V and VI, and the clamped dielectric constants shown in Fig. 8. The relative errors between f_{cal} and f_{meas} corresponding to all the modes in Table III are less than 0.3%. Those corresponding to all the modes in Table IV are less than 0.5%. This indicates that the constants $\{c_{11}^{\mathrm{E}},\ c_{12}^{\mathrm{E}},\ c_{13}^{\mathrm{E}},\ c_{33}^{\mathrm{E}},\ c_{44}^{\mathrm{E}},\ e_{15},\ e_{33}\}$ were precisely characterized because many resonance frequencies are sensitive to their variations [38]. Compared with these constants, most resonance frequencies are less sensitive to the piezoelectric constant e_{31}; therefore, the precision of e_{31} determined using RUS may be less than that of other constants determined using RUS. If there are no resonant modes that are sensitive to a specific constant, this constant cannot be precisely characterized using RUS. This is a disadvantage associated with the use of RUS for the characterization of PMs.

The elastic constants $\{c_{11}^{\mathrm{E}},\ c_{12}^{\mathrm{E}},\ c_{44}^{\mathrm{E}},\ c_{33}^{\mathrm{D}},\ c_{55}^{\mathrm{D}}\}$ of the rectangular parallelepiped PZT sample can be directly characterized by a high-precision UPE. Table VII lists their values characterized using UPE, RUS, and ER. The relative errors between the UPE and RUS results corresponding to $\{c_{11}^{\mathrm{E}}, c_{12}^{\mathrm{E}}, c_{44}^{\mathrm{E}}, c_{55}^{\mathrm{D}}\}$ are less than those between the UPE and ER

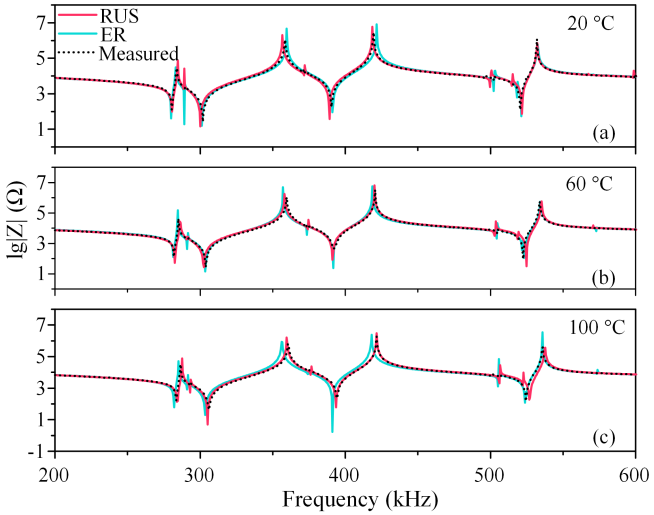

Fig. 9. Electrical impedance spectra measured by the impedance analyzer (black dashed lines) and calculated by using the FEM using the RUS (red solid lines) and ER (solid cyan lines) results from 200 to 600 kHz. (a) 20 °C, (b) 60 °C, and (c) 100 °C.

results. The relative error between the UPE and RUS results corresponding to c_{33}^{D} is greater than that between the UPE and ER results. Overall, the results obtained using RUS are better than those obtained using ER.

To compare the RUS and ER results, the electrical impedance spectra of the RUS sample in Table II were computed by FEM using the RUS and ER results and compared with those measured by the impedance analyzer from 200 to 600 kHz, as shown in Fig. 9. In Fig. 9, the black dashed lines represent the electrical impedance spectra measured using the impedance analyzer. The solid red and cyan lines are the electrical impedance spectra calculated from the RUS and ER results, respectively, using the commercial FEM software ABAQUS (Dassault Systèmes Simulia Corporation, Providence, RI, USA). They match each other. However, the electrical impedance spectra computed using the RUS results are more consistent with the measured spectra than those computed using the ER results at elevated temperatures.

Table VIII lists the third resonance and antiresonance frequencies f_{3r} and f_{3a}, and the fifth resonance and antiresonance frequencies f_{5r} and f_{5a} at 20 °C, 40 °C, 60 °C, 80 °C, and 100 °C. The maximum relative error between the measured $f_{3\mathrm{r}}$ and that computed from the RUS results is approximately 0.64% from 20 °C to 100 °C. Those corresponding to f_{3a}, f_{5r}, and f_{5a} are approximately 0.52%, 0.34%, and 0.20%, respectively. The maximum relative error between the measured $f_{3\mathrm{r}}$ and that computed from the ER results is approximately 0.79% from 20 °C to 100 °C. Those corresponding to f_{3a}, f_{5r}, and f_{5a} are approximately 1.22%, 0.85%, and 0.79%, respectively. Moreover, the relative errors between the measured $\{f_{3r}, f_{3a}, f_{5r}, f_{5a}\}$ and those computed from the ER results show an increasing trend with temperature, as shown in Table VIII. However, the relative errors between the measured $\{f_{3r}, f_{3a}, f_{5r}, f_{5a}\}$ and those computed from the RUS results do not exhibit significant variations as a function of temperature. Therefore, RUS is better than ER

TABLE VIII

RESONANCE AND ANTIRESONANCE FREQUENCIES $f_{3\mathrm{r}}$, $f_{3\mathrm{a}}$, $f_{5\mathrm{r}}$, AND $f_{5\mathrm{a}}$ (UNIT: KHZ) AT DIFFERENT TEMPERATURES

	T(°C)	20	40	60	80	100
	Measured	302.0	302.5	304.0	305.0	306.0
	RUS	300.1	301.6	302.6	303.6	305.1
f_{3r}	Relative error	0.64%	0.30%	0.47%	0.46%	0.30%
	ER	301.1	302.6	303.6	303.6	303.6
	Relative error	0.30%	0.03%	0.14%	0.46%	0.79%
	Measured	358.5	359.0	359.5	360.0	360.5
	RUS	356.6	357.6	358.1	359.1	359.6
f_{3a}	Relative error	0.52%	0.38%	0.38%	0.24%	0.24%
	ER	359.6	357.6	357.1	356.6	356.1
	Relative error	0.32%	0.38%	0.66%	0.94%	1.22%
	Measured	390.5	391.0	392.0	393.5	394.5
	RUS	389.2	390.2	391.2	392.2	393.7
f_{5r}	Relative error	0.34%	0.22%	0.21%	0.34%	0.21%
	ER	391.2	390.2	391.7	391.2	391.2
	Relative error	0.17%	0.22%	0.09%	0.60%	0.85%
	Measured	419.5	419.5	420.5	421.0	421.5
	RUS	418.7	419.7	420.2	420.7	421.7
f_{5a}	Relative error	0.20%	0.04%	0.08%	0.08%	0.04%
	ER	421.7	419.2	418.7	418.2	418.2
	Relative error	0.52%	0.08%	0.43%	0.67%	0.79%

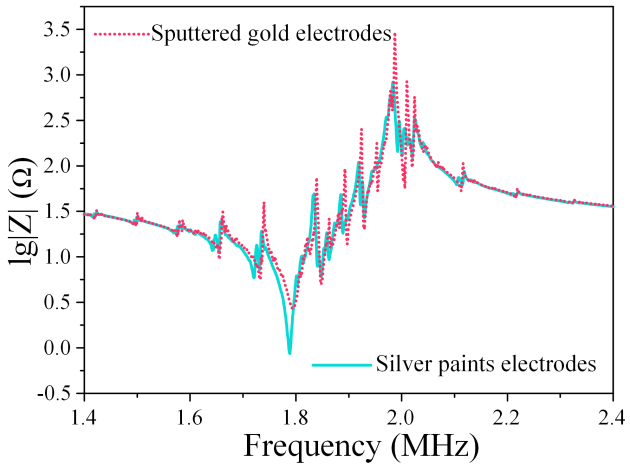

Fig. 10. Electric impedance curves of the TE resonator with different electrodes.

for characterizing the TD of the EPCs of the piezoelectric samples.

The accuracy of the ER results is influenced by many factors. The measurements of f_r and f_a constitute a key step in ER. The experimental results showed that the measurement was influenced by the force applied to the sample by the impedance testing fixture, clamping position, electrodes, and so on. Fig. 10 shows the electric impedance curves of the TE resonator with different electrodes. The red-dotted and

TABLE IX
COMPARISON BETWEEN RUS AND ER

	RUS	ER
Number of samples	Single	Multiple
Priori information of material constants	Necessary	Unnecessary
Sample sizes	No strict requirement	LTE: $l_x >> l_y$, $l_y >> l_z$ TE: $l_x >> l_z$, $l_y >> l_z$ RE: $r >> t$ TSE: $l_y >> l_x$, $l_z >> l_x$ LE: $l_z >> l_x$, $l_z >> l_y$
Requirement of Q_M	Above several hundreds [41]	No
Efficiency	RUS > ER	
Accuracy	RUS > ER	

solid cyan lines correspond to the samples with sputtered gold and silver paint electrodes, respectively. There is a difference between the values of f_r corresponding to the samples with different electrodes, as shown in Fig. 10. It should be noted that during the ER characterization, only the minimal and maximal impedance frequencies f_n and f_m can be measured by the impedance analyzer. In the calculation, it was assumed that $f_r \approx f_n$ and $f_a \approx f_m$, and this caused errors in the characterization results.

E. RUS Versus ER

It needs to be emphasized that regardless of the method employed to characterize the full matrix constants of PMs, high-quality samples are the premise of the characterization. Without high-quality samples, there would be no reliable high-quality data. If a large sample-to-sample variance exists among the multiple samples used in the ER method, inconsistent results will be obtained. If the RUS sample is inhomogeneous, the identification of resonance modes from the measured resonant ultrasound spectra cannot be successfully performed.

A comparison between RUS and ER is presented in Table IX. Due to the size requirements of the samples used in ER, some PMs, such as $Bi_4Ti_3O_{12}$ ceramics [39], cannot be easily characterized precisely using ER. Moreover, to characterize the full tensorial properties of certain PMs, a combination of ER and UPE should be employed. For example, the RE resonator cannot be used to characterize the value of s_{12}^E of PMs with a 4-mm or mm^2 symmetry. Therefore, the combination of ER with UPE was employed to characterize the full matrix constants of the $[001]_c$ and $[011]_c$ poled relaxor-based ferroelectric single crystals [8], [40]. One of the factors that limit the application of RUS is that Q_M of the piezoelectric samples to be characterized should be sufficiently high. Typically, Q_M should take values greater than several hundred [41]. However, there have been no published reports on the exact lower limit of this value.

Multiple samples, each of which satisfies specific size requirements, are needed by ER. RUS only needs one sample in the characterization. All samples should be ground after they are cut from a big sample. Therefore, the preparation of samples used in ER is far more time-consuming than that of the RUS sample. In this study, the preparation of the ER samples requires approximately five times the time required for the preparation of the RUS sample. Moreover, the temperature-dependent ER measurement requires more than three times the time used in the RUS measurement. In addition, each sample should be placed into the temperature chamber to conduct temperature-dependent measurements. ER should take significantly more time than RUS to complete the temperature-dependent measurements. In this study, the temperature-dependent ER measurements required more than three times the time required for the RUS measurement. The data processing of RUS required more time than that of ER because the mode identification and inversion in RUS were time-consuming. Overall, RUS is more efficient than ER according to our experience.

Moreover, it can be inferred based on the above discussion that the results determined using RUS are more accurate than those determined using ER. Notably, ER can only be used to characterize the material constants of PMs. However, in theory, RUS can be used to characterize the material constants of all solid materials with a sufficiently high Q_M, for example, elastic, piezoelectric, and piezomagnetic materials.

IV. CONCLUSION

The values of the material constants $\{s_{11}^E, s_{12}^E, s_{13}^E, s_{33}^E, s_{44}^E, d_{15}, d_{31}, d_{33}\}$ (except d_{31}) characterized using RUS are consistent with those characterized using ER, i.e., the relative errors between the RUS and ER results are less than 5% from 20 °C to 110 °C. The values of the material constants $\{c_{11}^E, c_{12}^E, c_{13}^E, c_{33}^E, c_{44}^E, e_{15}, e_{31}, e_{33}\}$, except e_{31} characterized using RUS, are consistent with those characterized using ER over the entire temperature range. The values of the material constants $\{k_{15}, k_{31}, k_{33}, k_t\}$, except k_{31} characterized using RUS, are in agreement with those characterized using ER over the entire temperature range. It is challenging to develop some new methods for improving the characterization accuracy of k_{31}, d_{31}, and e_{31} because neither ER nor RUS can characterize them with high accuracy.

The values of elastic constants $\{c_{11}^E, c_{12}^E, c_{44}^E, c_{33}^D, c_{55}^D\}$ at 20 °C determined using ER and RUS were compared with those determined using UPE. Moreover, the electric impedance spectra at different temperatures computed by FEM using the ER and RUS results were compared with those measured directly using the impedance analyzer. EPCs characterized using RUS are more accurate than those characterized using ER. In addition, RUS is more efficient than ER for characterizing the TD of the material constants of piezoelectric samples.

Before the application of RUS, ER was the only method available for the characterization of the TD of EPCs of PMs. Although it is important to assess the metrics of different methods, such as precision, efficiency, and limitations, there

is no published comparison of the ER and RUS techniques. In this study, a comprehensive comparison of the ER and RUS techniques for characterizing the TD of EPCs of PMs was performed based on the characterization process and results of Fuji C-213 PZT. The results obtained here provide a reference for the selection of various methods for characterizing the TD of EPCs of PMs.

REFERENCES

[1] R. Kazys et al., "High temperature ultrasonic transducers for imaging and measurements in a liquid Pb/Bi eutectic alloy," *IEEE Trans. Ultrason., Ferroelectr., Freq. Control*, vol. 52, no. 4, pp. 525–537, Apr. 2005.

[2] *IEEE Standard on Piezoelectricity*, ANSI/IEEE Standard 176-1987, 1988.

[3] M. Shanthi, L. C. Lim, K. K. Rajan, and J. Jin, "Complete sets of elastic, dielectric, and piezoelectric properties of flux-grown [011]-poled $Pb(Mg_{1/3}Nb_{2/3})O_3$-(28–32)% $PbTiO_3$ single crystals," *Appl. Phys. Lett.*, vol. 92, no. 14, Apr. 2008, Art. no. 142906.

[4] V. Y. Topolov, "Comment on 'complete sets of elastic, dielectric, and piezoelectric properties of flux-grown [011]-poled $Pb(Mg_{1/3}Nb_{2/3})O_3$-(28–32)% $PbTiO_3$ single crystals' [Appl. Phys. Lett. 92, 142906 (2008)]," *Appl. Phys. Lett.*, vol. 96, no. 19, May 2010, Art. no. 196101.

[5] X. Liu, S. Zhang, J. Luo, T. R. Shrout, and W. Cao, "Complete set of material constants of $Pb(In_{1/2}Nb_{1/2})O_3$–$Pb(Mg_{1/3}Nb_{2/3})O_3$–$PbTiO_3$ single crystal with morphotropic phase boundary composition," *J. Appl. Phys.*, vol. 106, no. 7, Oct. 2009, Art. no. 074112.

[6] E. Sun, S. Zhang, J. Luo, T. R. Shrout, and W. Cao, "Elastic, dielectric, and piezoelectric constants of $Pb(In_{1/2}Nb_{1/2})O_3$–$Pb(Mg_{1/3}Nb_{2/3})O_3$–$PbTiO_3$ single crystal poled along [011]c," *Appl. Phys. Lett.*, vol. 97, no. 3, Jul. 2010, Art. no. 032902.

[7] J. H. Yin, B. Jiang, and W. W. Cao, "Elastic, piezoelectric, and dielectric properties of 0.955$Pb(Zn_{1/3}Nb_{2/3})O_3$-0.045$PbTiO_3$ single crystal with designed multidomains," *IEEE Trans. Ultrason., Ferroelectr., Freq. Contr.*, vol. 47, no. 1, pp. 285–291, Jan. 2000.

[8] R. Zhang, B. Jiang, and W. Cao, "Elastic, piezoelectric, and dielectric properties of multidomain 0.67$Pb(Mg_{1/3}Nb_{2/3})O_3$–0.33$PbTiO_3$ single crystals," *J. Appl. Phys.*, vol. 90, no. 7, pp. 3471–3475, Oct. 2001.

[9] S. Sherrit, H. D. Wiederick, and B. K. Mukherjee, "Complete characterization of the piezoelectric, dielectric, and elastic properties of Motorola PZT 3203 HD, including losses and dispersion," *Proc. SPIE*, vol. 3037, pp. 158–169, Apr. 1997.

[10] S. Sherrit, T. J. Masys, H. D. Wiederick, and B. K. Mukherjee, "Determination of the reduced matrix of the piezoelectric, dielectric, and elastic material constants for a piezoelectric material with C_∞ symmetry," *IEEE Trans. Ultrason., Ferroelectr., Freq. Control*, vol. 58, no. 9, pp. 1714–1720, Sep. 2011.

[11] S. Zhang, S.-M. Lee, D.-H. Kim, H.-Y. Lee, and T. R. Shrout, "Temperature dependence of the dielectric, piezoelectric, and elastic constants for $Pb(Mg_{1/3}Nb_{2/3})O_3$–$PbZrO_3$–$PbTiO_3$ piezocrystals," *J. Appl. Phys.*, vol. 102, no. 11, Dec. 2007, Art. no. 114103.

[12] L. Qiao et al., "Temperature dependence of elastic, piezoelectric, and dielectric matrixes of [001]-poled rhombohedral PIN-PMN-PT single crystals," *IEEE Trans. Ultrason., Ferroelectr., Freq. Control*, vol. 66, no. 11, pp. 1786–1792, Nov. 2019.

[13] Z. Q. Zhuang, M. J. Haun, S.-J. Jang, and L. E. Cross, "Composition and temperature dependence of the dielectric, piezoelectric and elastic properties of pure PZT ceramics," *IEEE Trans. Ultrason., Ferroelectr., Freq. Control*, vol. 36, no. 4, pp. 413–416, Jul. 1989.

[14] S. Sherrit, G. Yang, H. D. Wiederick, and B. K. Mukherjee, "Temperature dependence of the dielectric, elastic and piezoelectric material constants of lead zirconate titanate ceramics," in *Proc. Struct. Syst.*, 1999, pp. 121–126.

[15] R. G. Sabat, B. K. Mukherjee, W. Ren, and G. Yang, "Temperature dependence of the complete material coefficients matrix of soft and hard doped piezoelectric lead zirconate titanate ceramics," *J. Appl. Phys.*, vol. 101, no. 6, Mar. 2007, Art. no. 064111.

[16] F. Li, Z. Xu, X. Wei, and X. Yao, "Temperature- and DC bias field-dependent piezoelectric effect of soft and hard lead zirconate titanate ceramics," *J. Electroceram.*, vol. 24, no. 4, pp. 294–299, Jun. 2010.

[17] M. Marutake and T. Ikeda, "Anisotropy in polarized barium titanate ceramics," *J. Phys. Soc. Jpn.*, vol. 12, no. 3, pp. 233–240, Mar. 1957.

[18] R. T. Smith and F. S. Welsh, "Temperature dependence of the elastic, piezoelectric, and dielectric constants of lithium tantalate and lithium niobate," *J. Appl. Phys.*, vol. 42, no. 6, pp. 2219–2230, May 1971.

[19] F. Chen, C. Jiang, F. Yu, X. Cheng, and X. Zhao, "Temperature-dependent behaviours of electro-elastic constants for the $Bi_2ZnB_2O_7$ piezoelectric crystal," *CrystEngComm*, vol. 23, no. 2, pp. 391–396, 2021.

[20] F. Ren et al., "The high-temperature elastic moduli of polycrystalline PbTe measured by resonant ultrasound spectroscopy," *Acta Mater.*, vol. 56, no. 20, pp. 5954–5963, Dec. 2008.

[21] M. J. Vaughan, K. van Wijk, D. J. Prior, and M. H. Bowman, "Monitoring the temperature-dependent elastic and anelastic properties in isotropic polycrystalline ice using resonant ultrasound spectroscopy," *Cryosphere*, vol. 10, no. 6, pp. 2821–2829, Nov. 2016.

[22] B. R. Goodlet, S. P. Murray, B. Bales, J. Rossin, C. J. Torbet, and T. M. Pollock, "Temperature dependence of single crystal elastic constants in a CoNi-base alloy: A new methodology," *Mater. Sci. Eng. A*, vol. 803, Jan. 2021, Art. no. 140507.

[23] R. Tarumi, T. Matsuhisa, and Y. Shibutani, "Low temperature elastic constants and piezoelectric coefficients of $LiNbO_3$ and $LiTaO_3$: Resonant ultrasound spectroscopy measurement and lattice dynamics analysis," *Jpn. J. Appl. Phys.*, vol. 51, no. 7S, Jul. 2012, Art. no. 07GA02.

[24] L. Tang and W. Cao, "Temperature dependence of self-consistent full matrix material constants of lead zirconate titanate ceramics," *Appl. Phys. Lett.*, vol. 106, no. 5, Feb. 2015, Art. no. 052902.

[25] L. Tang, H. Tian, Y. Zhang, and W. Cao, "Temperature dependence of dielectric, elastic, and piezoelectric constants of [001]c poled Mn-doped 0.24$Pb(In_{1/2}Nb_{1/2})O_3$-0.46$Pb(Mg_{1/3}Nb_{2/3})O_3$-0.30$PbTiO_3$ single crystal," *Appl. Phys. Lett.*, vol. 108, no. 8, Feb. 2016, Art. no. 082901.

[26] J. Hu, H. Fan, S. Wu, L. Tang, L. Qin, and W. Luo, "Characterization of temperature dependence of dielectric, elastic and piezoelectric properties of $BaTiO_3$ ceramics," *Ceram. Int.*, vol. 48, no. 18, pp. 25741–25746, Sep. 2022.

[27] N. G. Fenu, N. Giles-Donovan, M. R. Sadiq, and S. Cochran, "Full set of material properties of lead-free PIC 700 for transducer designers," *IEEE Trans. Ultrason., Ferroelectr., Freq. Control*, vol. 68, no. 5, pp. 1797–1807, May 2021.

[28] S. Bouchy, R. J. Zednik, and P. Bélanger, "Characterization of the elastic, piezoelectric, and dielectric properties of lithium niobate from 25 °C to 900 °C using electrochemical impedance spectroscopy resonance method," *Materials*, vol. 15, no. 13, p. 4716, Jul. 2022.

[29] *Test Methods for the Properties of Piezoelectric Ceramics Test for Poisson's Ratio* σ^E, National Standards of China GB 11311-1989, Ministry of Mechanical and Electronic Industry, Beijing, China, 1988.

[30] *IRE Standards on Piezoelectric Crystals: Measurements of Piezoelectric Ceramics-1961*, IEEE Standard 179-1961 (ANSI C83.24-1962), Jul. 1961.

[31] J. G. Smits, "Iterative method for accurate determination of the real and imaginary parts of the materials coefficients of piezoelectric ceramics," *IEEE Trans. Sonics Ultrason.*, vol. SU-23, no. 6, pp. 393–401, Nov. 1976.

[32] A. Migliori and J. L. Sarrao, *Resonant Ultrasound Spectroscopy: Applications to Physics, Materials Measurements, and Nondestructive Evaluation*. New York, NY, USA: Wiley, 1997, pp. 35–58.

[33] I. Ohno, "Rectangular parallellepiped resonance method for piezoelectric crystals and elastic constants of alpha-quartz," *Phys. Chem. Minerals*, vol. 17, no. 5, pp. 371–378, Dec. 1990.

[34] K. Madsen, H. B. Nielsen, and O. Tingleff, *Methods for Non-Linear Least Squares Problems*, 2nd ed. Lyngby, Denmark: Informatics and Mathematical Modelling, Technical Univ. of Denmark, 2004.

[35] J. Pujol, "The solution of nonlinear inverse problems and the Levenberg–Marquardt method," *Geophysics*, vol. 72, no. 4, pp. W1–W16, Jul. 2007.

[36] W. Yang et al., "Deep learning model as an inversion tool for resonant ultrasound spectroscopy of piezoelectric materials," *Appl. Phys. Lett.*, vol. 120, no. 18, May 2022, Art. no. 184101.

[37] J. J. Moré, B. S. Garbow, and K. E. Hillstrom, "User guide for MINPACK-1," Argonne Nat. Lab., emont, IL, USA, Tech. Rep. ANL-80-74, 1980.

[38] H. Li et al., "Characterizing elastic and piezoelectric constants of piezoelectric materials from one sample using resonant ultrasound spectroscopy," *J. Mater. Sci.*, vol. 54, no. 9, pp. 6786–6798, May 2019.

[39] W. Wang, K. Zheng, S. Sun, L. Qin, L. Tang, and Z. Li, "Characterization of the full matrix constants of $Bi_4Ti_3O_{12}$ ceramics," *Ceram. Int.*, vol. 47, no. 16, pp. 23518–23527, Aug. 2021.

[40] G. Liu, W. Jiang, J. Zhu, and W. Cao, "Electromechanical properties and anisotropy of single- and multi-domain $0.72Pb(Mg_{1/3}Nb_{2/3})O_3$-$0.28PbTiO_3$ single crystals," *Appl. Phys. Lett.*, vol. 99, no. 16, Oct. 2011, Art. no. 162901.
[41] F. F. Balakirev, S. M. Ennaceur, R. J. Migliori, B. Maiorov, and A. Migliori, "Resonant ultrasound spectroscopy: The essential toolbox," *Rev. Sci. Instrum.*, vol. 90, no. 12, Dec. 2019, Art. no. 121401.

Ailing Xiao received the B.S. degree in marine science from the China University of Geosciences, Beijing, China, in 2018. She is currently pursuing the Ph.D. degree with the Department of Applied Marine Physics and Engineering, Xiamen University, Xiamen, China.

Her research interests include the characterization of the temperature dependencies of real and complex full matrix material constants of piezoelectric materials.

Liguo Tang received the B.S. degree in physics from the Ocean University of Qingdao, Qingdao, China, in 1995, and the Ph.D. degree in acoustics from Nanjing University, Nanjing, China, in 2004.

From 2004 to 2005, he was a Research Assistant at the Department of Mechanical Engineering, Hong Kong Polytechnic University, Hong Kong. Currently, he is a Professor of applied marine physics and engineering and a Professor at the Key Laboratory of Underwater Acoustic Communication and Marine Information Technology, Xiamen University, Xiamen, China. His research interests include the characterization of piezoelectric materials and guided waves in multilayered media.

Shanshan Sun received the M.S. degree in marine physics from Xiamen University, Xiamen, China, in 2019, where she is currently pursuing the Ph.D. degree with the Department of Applied Marine Physics and Engineering.

Her research interests include the characterization of piezoelectric materials with low-mechanical quality factors.

Songji Wu was born in Guangdong, China, in 1996. He received the B.E. degree in electronics from Sun Yat-sen University, Guangdong, China, in 2019, and the M.S. degree in marine physics from Xiamen University, Xiamen, Fujian, China, in 2022.

His research interests include the development of scientific instruments for the characterization of materials.

Xinye Wu received the B.E. degree in mechanical engineering from the Central South University of Forestry and Technology, Changsha, China, in 2002, and the Ph.D. degree in mechanical engineering from Xiamen University, Xiamen, China, in 2013.

Currently, he is an Associate Professor of civil engineering at Xiamen University. His research interests include structural safety and evaluation, and the characterization of engineering materials.

Wenyu Luo was born in Sanhe, Hebei, China, in 1972. He received the B.S. degree in physics from the Ocean University of Qingdao, Qingdao, China, in 1995, and the Ph.D. degree in oceanographic engineering from the Massachusetts Institute of Technology, Cambridge, MA, USA, in 2007.

He is a Researcher at the Institute of Acoustics, Chinese Academy of Sciences, Beijing, China. His current research interests include wave propagation in layered media and the application of piezoelectric materials.